Thermal Kinetics of SiCp Reinforced Al-Zn-Mg-Cu Alloy Composite

Saikat Das
Tripura University

R. Govinda Rao
Sarada Institute of Science Technology and Management

Prasanta Kumar Rout (prasantarout@tripurauniv.in)
Tripura University https://orcid.org/0000-0002-6994-9260

Research Article

Keywords: AA7075, AA7075-SiCp composite, aging behavior, DSC, Activation energy, HRTEM.

Posted Date: April 19th, 2021

DOI: https://doi.org/10.21203/rs.3.rs-401141/v1

Version of Record: A version of this preprint was published at Silicon on August 17th, 2021. See the published version at https://doi.org/10.1007/s12633-021-01311-0.

Thermal kinetics of SiCp reinforced Al-Zn-Mg-Cu alloy composite

Saikat Das[1], R. Govinda Rao[2], Prasanta Kumar Rout[1]

[1]Tripura University (A Central University), Suryamaninagar, Tripura, India, 799022
[2]SISTAM Engineering Collage, Srikakulam, Andhra Pradesh, India, 532404

Corresponding author:

Dr. Prasanta Kumar Rout
Assistant Professor
Department of Material Science & Engineering,
Tripura University (A Central University),
Suryamaninagar-799022, Tripura (W), India
Contact: +91-7077567105
Email: prasantarout@tripurauniv.in

Thermal kinetics of SiCp reinforced Al-Zn-Mg-Cu alloy composite

Saikat Das[1], R. Govinda Rao[2], Prasanta Kumar Rout[1],
[1]Tripura University (A Central University), Suryamaninagar, Tripura, India,799022
[2]SISTAM Engineering Collage, Srikakulam, Andhra Pradesh, India, 532404
[1]Email: saikat.msen@tripurauniv.in

Abstract

In the present work, the artificial aging kinetics of SiCp particles reinforced AA7075-SiCp composite fabricated by stir casting method was investigated. The aging behavior of AA7075-SiCp composite was investigated by Rockwell hardness tests and differential scanning calorimetry (DSC). Results show there are no changes in the sequences of formation and dissolution of precipitate. Reinforced particles are uniformly distributed throughout the matrix. The hardness profile shows increase in hardness with the comparison of AA7075 base alloy. In addition to SiCp in the matrix, precipitation kinetics has changed compared with base alloy since higher dislocations present in composite, hence requires lower activation energy to form ή precipitate and takes less time to reach the maximum hardness. In contrast, the addition of SiCp at low volume percent also showing accelerated aging phenomena in the composite during the aging process. High-resolution transmission electron microscope (HRTEM) micrograph of peak age (T6) condition divulges that enormous fine and plate-like ή ($MgZn_2$) precipitates are uniformly distributed in the composite.

Keywords: AA7075, AA7075-SiCp composite, aging behavior, DSC, Activation energy, HRTEM.

1. Introduction

Aluminum matrix composite (AMCs) has drawn remarkable attentions because of its superior properties like high strength, good wear resistance, high specific modulus These attractive properties make the AMCs as a candidate material for application in the field of aerospace as well as automobile industries [1]. An enormous number of investigations have been carried out on AMCs to improve properties and increase application. The precipitation sequence of aluminum alloy is as follows: α - supersaturated solid solution (α - ssss) → GP zones (Zn, Mg) →ή ($MgZn_2$) → η ($MgZn_2$). Thermal treatment is the most significant method to increase the application area of AMCs which are based on precipitation hardening phenomenon [2-5]. Inspection showed that reinforcement in AMCs does not affect the sequence of precipitation formation but changes the precipitation kinetics of AMCs during the aging process [6, 7]. Inception of ceramic particles in the matrix alloys introduced enormous dislocations to the immediate vicinity of the reinforcement. Generation of these dislocations in the matrix is due to the mismatch of coefficient of thermal expansion (CTE) between the matrix and reinforcement when specimens are cool down rapidly from higher to lower temperature. These dislocations act as high diffusivity tracks and nucleation spots of Guinier- Preston (GP) zones, precipitates or different intermediate phases

Most researchers have focused their studies on aluminum-based AMCs reinforced with Al_2O_3, SiC, Si_3N_4, and TiC, etc. [6,8–10]. Among them, silicon carbide (SiC) particles have higher strength, high wear resistance, excellent thermal shock resistance, and low thermal expansion coefficient [10-12]. There are several methods to manufacture AMCs such as powder metallurgy [13-15], squeeze casting [16], stir casting technique [17-19,1], friction stir welding [20,21] and spraying process [22, 23]. Wang et al. [24] showed that the addition of SiCp (15 vol. %) in the matrix alloy (AZ91) reduced the peak aging time to 28 hr, higher age hardening efficiency, and faster aging kinetics. Dasgupta et al. [19] found a significant

improvement in the hardness of 15 vol.% SiCp-AA7075 composite than that of AA7075 alloy. LEE et al. [25] reported that composite AA7075 with 10 vol.% of SiCp showed higher strength values in all aging conditions. Kumar et al. [26] found that AA7075-SiCp composite showed better mechanical properties with the addition of 2 wt% SiCp in the AA7075 matrix alloy. Bembalge et al. [27] reported that AA6063-SiC composite with 4 wt.% of SiCp showed age-hardening kinetics were accelerated and maximum hardening affect was observed at 150 ^{o}C. They attributed this behavior presence of enormous dislocations in the matrix due to mismatch of CTE between the alloy and SiCp. Review of existing scientific literature discovered that the addition of SiCp particles would affect the aging kinetics during the aging process. Evaluation of the process activation energy or thermal diffusion activation energy (TDAE) is the main key to understand the aging kinetics or transformation kinetics. Lu et al. [28] found that TDAE in the AA7075-SiCp composite is lesser than AA7075 alloy. They attributed this behavior to increase of dislocation densities in the composite by the addition of SiC particles. Similarly, Min et al. [29] reported that AA6061required higher activation energy to form β′ phases than that of 40 vol. % AA6061-SiCp composite. Jin et al. [10] reported that with increase in solution temperature, TDAE of GP zone formation and dissolution in the composite increases due to lower vacancy concentration at higher temperature. On the other hand thermal diffusion activation energy for S′ phase requires lower activation energy attributed higher vacancy concentration at higher temperature.

However, age hardening kinetics of composites during the aging treatment depends on matrix metal and reinforcing elements such as size, volume fraction, aging temperature etc. Small particles can load-transfer through the composite interface and achieve enhancement in the strength; while increasing the volume fraction, particles lose their ability to homogeneous distribution and ductility with strength. From the above discussion, it is clear that lots of investigation has done on aging behavior of AA7075-SiCp composite but not enough data

available to the evaluation of process activation energy or thermal diffusion activation energy required forming the phases like GP zone, metastable (ή) and stable (η) phases at lower volume fraction. So, in the present work, reinforcement was restricted to 5 vol. % of SiCp to retain their ductility with strength and fluidity of composite melt. Efforts have been made to understand the aging kinetics of AA7075-SiCp composite. The ageing behavior of the AA7075-SiCp composite was investigated by Rockwell hardness tests and differential scanning calorymetry (DSC). Microstructure of composite was examined by optical microscopy (OM), scanning electron microscopy (SEM) and high resolution transmission electron microscopy (HRTEM). Simultaneously, open circuit potential with time has been studied to understand the electrochemical behavior with aging.

2. Experimental procedure

2.1 Material

AA7075 alloy based metal matrix composites are prepared using stir casting route. The chemical composition is shown in Table 1. Alloy ingot is cut into small pieces and preheated in the muffle furnace up to 400^{o}C. These pieces are melted in bottom pouring furnace at 780^{o}C. Furnace is attached with the boron coated stainless steel stirrer. Stirrer is rotated at 650 rpm to create the vortex. Reinforcing agents (SiC) are also separately preheated in muffle furnace up to 600^{o}C to improve wettability. Particles are poured into vortex, stirrer is moved up and down with the clearance of 12mm for maintaining the uniform distribution of particles. Argon gas is continuously passed into the liquid melt during melting to avoid molten metal oxidation. Liquid metal poured into pre heated (150 ^{o}C) rectangular metal mould.

2.2 Microstructural Analysis

For microstructural analysis of the specimens, specimens were ground with 80 to 1500 emery paper followed by cloth polish using 0.5 µm diamond paste and etched with Keller's reagent (Distilled water 95%, HNO_3 2.5%, HCl 1.5%, HF 1%) to reveal grain and grain boundary. Optical microscope (OM) LEICA DM 750M and scanning electron microscope (SEM) ZEISS-SIGMA 300 were used to observe specimens' surface morphology.

For HRTEM study, samples were mechanically thin up to 40 µm followed by 3 mm diameter discs punched from foil, dimpling, and ion milling. To observed microstructural features, precipitates and second phase particles etc., HRTEM (JEM-2100, JEOL make, Japan) at 200kv was used.

2.3 Ageing behavior:

The alloy and composite's aging behavior was studied by solution treating them at 470 ^oC for 1 hour soaking period and followed by water quenching. After that, specimens were artificially aged at 120 ^oC for different time. Hardness measurement was carried out by digital Rockwell hardness testing machine (SSS instrument, India) at 100 kgf load, dwell time 10 second.

2.4 X-ray diffraction (XRD) analysis:

XRD of the base alloy and composite were taken using PANlytical X'pert pro Basic X-ray diffractometer unit CuKα radiation.

2.5 Differential scanning calorimetry (DSC) analysis

To identify the precipitation sequence of alloy and composite, DSC study were carried out. The specimens weight of 13 mg approx. were cut from the alloy and composite, solutionized at 470 ^oC for 1 hr soaking time followed by water quenching. DSC run were initiated at room temperature to 500 ^oC at various heating rates (5K, 10K, 15K, 20K, 25 K) to study the deviations in activation energy for precipitation using a NETZSCH DSC instrument

model 214polyma, Germany. As a reference sample pure aluminium was used and to nitrogen gas was flushed to suppress oxidation.

2.6 Open circuit potential with time (OCPT)

For OCPT, aged samples were mechanically ground with emery paper up to 1500 grade. Three (3) electrode systems were used for OCPT measurement where samples were working electrode, Ag and Ag/Cl as reference electrode. Platinum rod serves as counter electrode. OCPT has run for 6 hours in 3.5 wt.% of NaCl neutral solution. The electrochemical measurement was carried out on CHI660E, a product of CH instruments.

3. Results and discussion

3.1 Microstructural characteristics

Fig. 1 (a, b) shows the scanning electron micrograph (SEM) of silicon carbide (SiC) particles of sizes 30 µm (approx.). Fig. 1(c,d) shows energy dispersive X-ray (EDX) analysis of powders and confirms that powders are SiC. Fig. 1(e,f) shows the optical microstructure (OM), SEM micrograph of AA7075-5 Vol.% of SiC composite respectively with constant volume fraction, reveals no dendritic structure. Micrographs also see the composite consits of α-Al and depicts some considerable distribution of senond phases in the composite. Distribution of grains is uniform, clearly defined , no defects were found in the samples. SEM micrographs of AA7075-5 Vol.% of SiC composite reveal uniform distribution of grain and grain boundaries and the presence of secondary phases in the matrix. EDX point analysis (Fig. 1g) confirms the enrichment of solute item including Zn, Mg and Cu.

Fig. 8 shows HRTEM micrograph of AA7075-5 vol. % SiC composite reinforced by SiCp aged at 120 ºC for 24 hours were investigated to analyze precipitation morphology. It has been widely reported that the important precipitate in the alloy matrix after aging are η′ phases [30, 31]. HRTEM morphological study reveals that enormous fine (approx. 100 nm)

and plate-like ή precipitates are uniformly distributed in the composite at peak age condition (Fig. 1a). Fig. 1d shows the corresponding electron diffraction patterns of Al matrix. Fig. 1b represents precipitates present in the grain boundaries. Most of the dislocations are still present in the matrix after aging treatment since the aging temperature 120 ^{o}C was not high enough to properly annihilate the dislocations. Fig. 1c reveals the dislocation present near the interface between matrix and SiCp particle. This behavior is attributed to the large differences in Co-efficiency of thermal expansion (CTE) matrix and reinforcement.

The CTE for SiCp and AA7075 are 4.7×10^{-6}/°C and 23.6×10^{-6}/°C (25–100 °C) respectively. When sample is solutionized and quenched, solute atoms are dissolved in the solid solution and internal strains are completely relieved and lead to the formation of enormous number of high density dislocations. At the time of ageing treatment at a temperature of 120 ^{o}C, this temperature gives a motivating force for transmission of precipitates mostly ή phase. These precipitates particles acts as an obstacle movements of dislocations, in a results it reach to maximum strength.

3.2 Aging study and hardness measurement

Aging time as the function of hardness changes of unreinforced alloy and composite after the solution treatment at 470 ^{o}C. Fig. 2 shows the hardness changes for the unreinforced AA 7075 alloy and AA 7075- 5 vol. % SiC composite artificially aged at 120^{o}C. Table 2 shows Rockwell hardness (HRB) values for AA 7075 alloy and AA 7075 alloy- 5 vol % SiC composite aged at 120^{o}C. In the aging curve of AA7075 alloy base and composite, the under-aged (UA) hardening may be attributed due to the GP zones at the time of 0.5 hours of duration. The maximum hardness values for alloy and composite are 86 and 89 HRB at 120 ^{o}C aging temperature, respectively. It has been seen that AA7075 the specimens were reached at peak age (PA) condition 40 hours of duration at aging temperature 120^{o}C as shown in Fig. 2, which is agreed with previously published data [32, 17], whereas composite took 24 hours

to reach peak hardness. This suggested that adding SiC particle could quicken the aging kinetics of AA7075- 5 vol. % SiCp composite. Though composite takes less time to reach the peak hardness, indicating that aging kinetic is accelerating, the main noticeable is that the maximum hardness values of both alloy and composite are pretty similar. This is because of the less quantity of Mg atom in the Al matrix, responsible for the precipitation of strengthening phases like $MgZn_2$. It has previously been stated that aggregation of Mg elements at the matrix-reinforcement interface can affect ageing behaviour and mechanical properties [33-35]. Unreinforced alloy AA7075 showed a broad hardness peak, whereas composite shows a sharp peak; exhibits accelerated aging phenomena for composite. On further aging at the same temperature for long duration (120 hours), the hardness values gradually decrease. The hardness values at over age OA conditions are 83 and 81 for AA7075 and AA7075-5 vol. % SiCp composite, respectively. This OA hardening condition could be attributed to the stable η precipitate.

3.3 DSC analysis

Fig. 3 shows the DSC thermograms of as quench specimen AA7075 at various heating rates of 5K/min, 10K/min, 15K/min, 20K/min and 25 K/min. It shows several exothermic and endothermic peaks at different temperatures and indicates the formation and dissolution of precipitation. At lower heating rate, peaks are broader than that of higher heating rate i.e. with increasing the heating rate, exothermic and endothermic peaks are becoming sharp and shifted to higher temperature, indicating that the reactions are thermally affected. As per literature, exothermic peaks are associated with the formation of the precipitation phenomenon. Alternatively, the dissolution of precipitation phenomenon is related to endothermic peaks. Exothermic and endothermic peaks are marked with numerals I-VI and identified as: I- formation of GP zone, II- dissolution of GP zone, III- formation of ή ($MgZn_2$), IV- dissolution of ή ($MgZn_2$), V- formation of η ($MgZn_2$) phase, and VI-

dissolution of η ($MgZn_2$) phases. Formation and dissolution of GP zone at temperature interval of 70 ^oC to 170 ^oC at different heating rates, shows the kinetics of GP zone which are form during low temperature aging. Table 3 shows exothermic and endothermic peak temperatures of the as quench specimen of AA7075 at different heating rate. The peak temperature III and IV indicates the formation and dissolution of metastable phase (ή) precipitation from the temperature interval of 220-300^oC. Nucleation of metastable phase requires vacancies. From Table 3 peak temperature V and VI attributed with the formation and dissolution of η phase. It has been noticed that dissolution of η phase is broader than ή phase. This observation indicating that the absorption of energy during the dissolution of equilibrium phase (η) larger than that of metastable phases (ή).

Fig. 4 shows differential scanning calorimetry (DSC) curves of the as quench specimen of AA7075-SiC with 5 vol. % of SiCp composite at different heating rates. The composite also shows the many exothermic, endothermic peaks which are attributed to the formation and dissolution of GP zone, metastable phase (ή), and stable phase (η), respectively. Table 4 shows exothermic and endothermic peak temperatures of the as quench specimen of AA7075-5 Vol.% of SiC composite at various heating rates. Due to the mismatch of the coefficient of thermal expansion, introduce increase in dislocation density and vacancies and these vacancies are requires for the formation of GP zones.

On the other hand, deficiencies in vacancies or devoid do not nucleate GP zones, rather than giving spaces for precipitation nucleation. Fig 4 indicates that the precipitation sequence does not alter with the addition of a small amount of SiC particle, however, peak temperatures related to formation and dissolution of phases shifted at lower temperature, which indicating thermally affected with the addition of small quantity of SiC particle and also suggests that the activation energy for this transformation is lower. Peaks of exothermic temperatures are

sharp compared to unreinforced alloy and reduced, suggesting that formation of zones is significantly suppressed by addition of carbide.

The formation of precipitation in this alloy and composite with the GP zone, requires an access amount of vacancies, caused due to the mismatch of thermal coefficient. An increase in dislocation density may result in heterogeneous nucleation of precipitation and reduce the activation energy for precipitation. The sequences of precipitation of composite is identifies by inference with the unreinforced alloy. Shifting of DSC peak temperatures for ή precipitation of composite in lower temperature indicates that this transformation's activation energy is lower. Comparison of the DSC thermograms AA7075 has shallow peaks compared to AA7075-SiC composite, which indicates that volume fraction of those regions is larger, which requires more activation energy to transformation.

The dislocation density of the material is associated with the variations in alloy and composite ages [26]. Typically, mismatch strains happen because of differences of CTE among the matrix and reinforcement, while composite is cooled down from the solution temperature. The dislocation density (ρ) and mismatch strain (ε) can be calculated as revealed by Arsenault and Shi [9].

$$\varepsilon = \Delta\alpha \times \Delta T \qquad (1)$$

$$\rho = \frac{BV_f\varepsilon}{bt(1-V_f)} \qquad (2)$$

Where, $\Delta\alpha$ is the CTEs and ΔT is temperature gradient. Whereas, B, V_f, b, t are the geometric constant, volume fraction of reinforcement, burgers vector and smallest dimensions of the reinforcement respectively. Equation (1) reveals that higher the ΔT value and residual stress, higher the dislocation density [36]. Plastic deformation, strains occurs as a result of the thermal mismatch, resulting in a high density of dislocations, particularly near the SiC particulates. The dislocation density (ρ) can be evaluated by equation (2). The previous

research work [37] indicated that the growth of precipitates accelerated at the dislocations because dislocations create free path for the kinetically faster atomic transportation of precipitates comparative to majority transmission in a crystal. Hence, presence of SiC particles in the composite would offers a lot nucleation site of precipitate, resulting shorter in the aging time than that of the AA7075.

$$\ln\left[\frac{T_p^2}{Q}\right] = \frac{E}{RT_P} + \ln K \qquad (3)$$

$$\tan(\theta) = \frac{E}{R} \qquad (4)$$

Where,

T_p = Peak temperature of the formation of precipitates,

Q = Heating rate,

E = Thermal diffusion activation energy,

R= Gas constant (8.314 j/mol)

K = Reactive constant. To obtain the diffusion activation energy of the materials, the variation of $\ln\left[\frac{T_p^2}{Q}\right]$ and $1000/T_p$ are plotted. For calculating diffusion activation energy of GP zone, ή and η, calculated data are fitted and straight lines represents slope of E/R, in equations (3) and (4). Calculated activation energies are summarized in Fig. 5 (a)-(f). Table 5 shows the diffusion activation energies of AA7075 and AA7075-5 vol. % SiC composite. The required thermal diffusion activation energy of AA7075 alloy for formation of GP zone, ή and η for are 73.42, 127.53, 146.02 kJ/mol respectively. Whereas, formation of GP zone, ή and η precipitates for AA7075-SiC composite required thermal diffusion activation energies are 69.89, 117.65, 139.6 kJ/mol respectively. It is seen that AA7075-SiC composite required lower activation energy to form precipitates than AA7075. Differences in the activation

energy can be attributed to the reduced dislocations which are caused due to the mismatch of CTE [38]. From the previous research, it is clear that precipitates were nucleate at the dislocation to diminish their strain field through the matrix [39]. Although, growth of the phases has to competes with others to acquire solute atoms just because of limited solute particles in the matrix alloy. The AA7075 alloy's rational precipitate growth necessitates more activation energy for precipitate growth than the SiCp composite, resulting in a composite that is more sensitive to ageing temperature. The TDAE of composite is lower than AA7075, indicating that lower energy was required to form the phases, i.e. formation of phases is accelerated that can be attributed to excess nucleation sites provided by dislocations [28]. Therefore, faster the solute atoms diffuse, shorter the aging time to reach the peak aging hardness. Finally, AA7075-SiC composites reach peak aging time in shorter time than the matrix.

Fig. 6 shows the DSC thermograms of as-quenched (AQ), T4, T6, T7 tempers of AA7075 at a heating rate of 10 k/min. DSC curve has showing temperature effect at a constant heating rate. AQ sample has showing many exothermic and endothermic peak temperatures with increasing the temperature which are associated with formation and dissolution of phases GP zone, η′ phase, η phases etc. marked with numerals (*I-II), (III-IV),(V-VI)* respectively. Two distinct doublet exothermic peaks have shown at the temperature interval of 190 ^{o}C to 250 ^{o}C. First peak is associated with formation of η′ precipitate and second peak is associated with the transformation of η′precipitate into stable η precipitate. For AA7075-T4 temper a broad endothermic peak at 146 ^{o}C which is associated with dissolution of GP zone. Whereas other exothermic and endothermic peak positions of AA7075-T4 temper are much similar to the AQ sample, the temper is more supersaturated. In the case of AA7075- T6 and AA7075-T7 temper at lower temperature, these alloy tempers are not showing any exothermic and endothermic peak, i.e., zone I and II are vanished

associated with GP zone formation, implies tempers are not more supersaturated with solute atoms. With increasing the aging time this endothermic peak temperature has shifted to higher temperature (for temper T6 and T7) at temperature of 194 – 198 ^{o}C respectively. This peak associated with the dissolution of GP zone and η′ precipitates, which are already existed saturated level of η′ precipitates. A sharp exothermic peak at temperature 228^{o}C and 231 ^{o}C of AA7075- T6 and AA7075-T7 tempers respectively demonstrates the transformation of η′ precipitate into stable η precipitate. The exothermic peak for η precipitation at the temperature 268 ^{o}C for AA7075-T7 temper is much broader then AA7075-T6 temper. But the noticeable thing is that for AA7075-T7 temper transformation peak from ή to η is still present in overage temper. It can be ascribed, for transformation of phases from one to another requires a higher driving force and this aging temperature acts as a driving force. Higher the aging temperature higher the driving force and lower the aging time. In this case, the aging temperature 120 ^{o}C is not high enough to transform the η′ into η within the 120 hours of duration i.e. it requires more time to completely transform into η precipitate. The final broad endothermic peak region of all tempers is associated with the dissolution of equilibrium η precipitates.

Fig. 7 shows the DSC thermograms of as-quenched (AQ), T4, T6, T7 tempers of AA7075-5 vol. % SiC particulate composite at a heating rate of 10 k/min. As the same for the composite also graph showing many exothermic and endothermic peak temperature which is distinguish by formation and dissolution of phases GP zone, η′ phase, η phases etc. marked with numerals (*I-II), (III-IV),(V-VI)* respectively. The composite of T4 temper shows a broad endothermic peak at lower temperature which is attributed to the dissolution of GP zone and with increasing the time this endothermic reaction peak has shifted to higher temperature of 189 ^{o}C and 194 ^{o}C for T6 and T7 temper. It is clear that aging kinetics is thermally affected due to addition of SiCp in the matrix and decreased the aging time. An exothermic peak

temperature at interval of 229 ºC – 231ºC of tempers are associated with the transformation of metastable ή precipitate into stable η precipitate. Adjacent two peaks (endothermic and exothermic) of this transformation peak (ή →η) are attributed by dissolution of metastable and formation of stable η phase. And finally, the broad endothermic peak marked with *IV* (compared with AQ) is associated with the dissolution of the stable η phase.

3.4 XRD studies

Fig. 9 shows the XRD patterns of AA7075 and AA7075- SiC 5 vol. % composite of as cast sample, illustrates the phase analysis of AA7075 and AA7075- SiC. AA7075 contains Al, $MgZn_2$ phases, whereas AA7075-SiC contains Al, SiC and $MgZn_2$ phases. This indicates the SiC particles are preserved in the composite. The presence of $MgZn_2$ in the alloy and composite identified by XRD analysis revealed that formation of fine $MgZn_2$ precipitate in all peaks related to peak hardness of alloy composite.

3.5 Open circuit potential (OCP) studies

Fig. 10 shows the variation of open circuit potential with time of (a) AA7075 (b) AA7075- SiC 5 vol. % composite of various tempers immersed in 3.5 Wt. % NaCl solutions for a period of 6 hours. As compared to alloy tempers at the same stage of immersion, composite tempers showed sudden increase in voltage at the beginning for a shorter time period and after some time it will stabilize with prolongation of dipping time (Fig. 10b). This can be ascribed by the formation of passive layer on the surface of the composite. Fig. 10 (a,b) shows electrochemical noise (EN) amplitude of the base alloy tempers are higher than that of composite tempers. As the same for other composite tempers, fluctuations had seen but less than AQ specimen (Fig. 10b). This fluctuation can be characterized by the free corrosion potential of the material i.e. variations in cathodic or anodic process in a system causes fluctuations in corrosion potential. Anodic process can be ascribed as dissolution of

aluminium alloy occurs due to the breakdown of passive film as a result of a potential drop to a negative position. On the other hand, passive film has the recovering ability which leads the potential drop to positive position. In the aluminum alloy matrix, the anodic particles are Al, Mg and the cathodic particles are Cu, Mn, and Zn which creates galvanic couples in the aqueous solution when immerged. Therefore, these galvanic actions are mainly responsible for breakdown of passive film, resulting in corrosion of material. As compared to alloy, composite shows shifting of OCP values towards noble direction. Because SiC particles are nonmetallic in nature and acts as inert component in the composite. So, when composite dipped into the electrolyte SiC particles reduces the effective corrosion unit area, as results less area for corrosion and shifting of OCP values towards noble direction. On the other hand, composite has less galvanic couple according to alloy. This will effect on the amplitude of the EN measurements. Each galvanic couple has their own electrode potential and this variations in potential will superimposed with into the fluctuations causes variations in amplitude. As compared to alloy, composite has less second phases in unit area, form less galvanic corrosion cells on the surface. Therefore, EN amplitude of composite will less than that of alloy.

Fig. 10 (a,b) indicates that the OCP have shifted towards noble direction from under age to over-aged temper. The reduction of Mg can ascribe it, Zn contents in the solid solution and formation of anodic η ($MgZn_2$) precipitates upon artificial ageing. For the AQ temper, the potential values is much lower, this can be attributed by the breakdown of single- phase solid solution, homogenization solution. This breakdown caused due to the presence of Mg and Zn into the solid solution. With increasing the aging time, the amount of Mg and Zn are reduces because of formation of precipitates $MgZn_2$ and the OCP values shifted to noble direction.

4. Conclusion

In summary, the incorporation of SiC particles in the matrix alloy has significant influences on the aging behavior of AA7075- SiC composite produced by stir casting method. Results showed that addition of SiC particles does not alter the precipitation sequence whereas it accelerate the aging time of AA7075-SiCp composite approximately 16 hours prior in comparison with AA7075, attributed to the increased in nucleation sites and lower the activation energy of ή precipitation. Additionally, variations in the hardness of AA7075 and AA7075-SiC composite at 120 ^{o}C for varying time attributed the precipitation phenomena and attained maximum hardness at 24 hours and 40 hours. From the experimental results, it can be concluded that the precipitate's activation energy for composite is smaller than matrix alloy. The CTE imbalance between the reinforcement and matrix alloy results in a large number of dislocations adjacent to the ceramic phase. These dislocations serves as high diffusivity route and nucleation sites for precipitates as a result takes less time to grow the precipitate as well as to reach the peak hardness. TEM morphological study at peak age condition also revealed, specimen were fully uniformly distributed with precipitate. Composites show better electrochemical behavior in 3.5 wt. % of NaCl solution with aging than that of unreinforced alloy.

Acknowledgements

The authors are very much thankful to the technical staffs of Central Research Facility (CRF), IIT Kharagpur, India for allowing us to avail the TEM and Central Instrumentation Center (CIC), Tripura University (A Central University), India for allowing us to avail the SEM facility.

Authors' Contributions All of contributors is in the author's list.

Availability of Data and Material: All of data and material are available.

Code Availability Not applicable

Declarations The manuscript is in compliance with ethical standards.

Conflict of Interest No conflict of interest in this study.

Consent to Participate All of the authors confirms the consent to participate.

Consent for Publication All of the authors confirms the consent for Publication.

References:

[1] R. K. Bhushan, S. K., S. Das (2013) Fabrication and characterization of 7075 Al alloy reinforced with SiC particulates. Int J Adv Manuf Technol 65:611–624

[2] H.Y. Yue , J. Chang, X. Gao, S. L. Zhang, J. J. Zhang, H. Zhang, W. D. Fei , Z. M. Yu, E.J. Guo , F. W. Kang, L. P. Wang (2014) Effects of ZnO coating of whiskers on the tensile properties and aging behaviors of aluminum borate whiskers reinforced 2024 Al composite. Mater Sci Eng A 607:89–94

[3] D. Mandal, S. Viswanathan (2013) Effect of heat treatment on microstructure and interface of sic particles reinforced 2124 al matrix composite. Mater Charact 85:73–81

[4] G. Das, M. Das, S. Ghosh, P. Dubey, A. K. Ray (2010) Effect of aging on mechanical properties of 6063 Al-alloy using instrumented ball indentation technique. Mater Sci Eng A 527:1590–1594

[5] W. H. Yuan, B. L. An (2012) Effect of heat treatment on microstructure and mechanical property of extruded 7090/SiCp composite. Trans Nonferrous Met Soc China 22:2080 –2086

[6] G.Q. Chen, W. S. Yang, K. Ma, M. Hussain, L. T. Jiang, G. H. Wu (2011) Aging and thermal expansion behavior of Si_3N_4p/2024Al composite fabricated by pressure infiltration method. Trans Nonferrous Met Soc China 21:S262–S273

[7] M.M. Sharma, M. F. Amateau, T. J. Eden (2006) Aging response of Al–Zn–Mg–Cu spray formed alloys and their metal matrix composites. Mater Sci Eng A 424:87–96

[8] A. Sahin, F. Sarioglu (1997) Effect of reinforcements on precipitation behavior in al 7075/TiCp composite. Scr Mater 37:1117–1121

[9] H.S. Chu, K. S. Liu, J.W. Yeh (2001) Aging behavior and tensile properties of 6061Al-0.3μm Al_2O_3 particle composite produced by reciprocating extrusion. Scr. Mater 45:541-546

[10] P. Jin, B. L. Xiao, Q. Z. Wang, Z. Y. Ma, Y. Liu, S. Li (2011) Effect of solution temperature on aging behavior and properties of SiCp/Al–Cu–Mg composites. Mater Sci Eng A 528:1504–1511

[11] Y. Du, P. Zhang, J. Zhang, S. Yao (2012) Radial distribution of SiC particles in mechanical stirring of A356–SiCp liquid. J Mater Sci Technol 28:951-955

[12] S. Bathula, M. Saravanan, A. Dhar (2012) Nano indentation and wear characteristics of Al 5083/SiCp nano composites synthesized by high energy ball milling and spark plasma sintering. J Mater Sci Technol 28:969-975

[13] H. Izadi, A. Nolting, C. Munro, D.P. Bishop, K.P. Plucknett, A.P. Gerlich (2013) Friction stir processing of Al/SiC composites fabricated by powder metallurgy. J Mater Process Technol 213:1900-1907

[14] C.Y. Sheu, S.J. Lin (1996) Particle size effects on the abrasive wear of 20 vol% SiC/7075Al composites. Scr Mater 35:1271-1276

[15] A. Ahmed, A.J. Neely, K. Shankar, P. Nolana, S. Moricca, T. Eddowes (2010) Synthesis, Tensile Testing, and Microstructural Characterization of Nanometric SiC Particulate-Reinforced Al 7075 Matrix Composites. Metall Mater Trans A 41:1582-1591

[16] A. Kalkanl, S. Yılmaz (2008) Synthesis and characterization of aluminum alloy 7075 reinforced with silicon carbide particulates. Mater Des 29:775-780

[17] M. Rajamuthamilselvan, S. Ramanathan (2012) Development of processing map for 7075 Al/20% SiCp composite. J Mater Eng Perform 21:191-196

[18] M.S. Rajamuthamil, S. Ramanathan (2013) Effect of silicon carbide volume fraction on the hot workability of 7075 aluminum-based metal–matrix composites. Int J Adv Manuf Technol 67:1711-1720

[19] R. Dasgupta, H. Meenai (2005) SiC particulate dispersed composites of an Al–Zn–Mg–Cu alloy: Property comparison with parent alloy. Mater Charact 54:438-445

[20] M. Bahrami, K. Dehghani, M. K. B. Givi (2014) A novel approach to develop aluminum matrix nano-composite employing friction stir welding technique. Mater Des 53:217-225

[21] M. Bahrami, N. Helmi, K. Dehghani, M. K. B. Givi (2014) Exploring the effects of SiC reinforcement incorporation on mechanical properties of friction stir welded 7075 aluminum alloy: fatigue life, impact energy, tensile strength. Mater Sci Eng A 595:173-178

[22] O. Meydanoglu, B. Jodoin, E.S. Kayali (2013) Microstructure, mechanical properties and corrosion performance of 7075 Al matrix ceramic particle reinforced composite coatings produced by the cold gas dynamic spraying process. Surf Coat Technol 235:08-116

[23] Y.H.F. Su, Y.C. Chen, C.Y.A. Tsao (2004) Workability of spray-formed 7075 Al alloy reinforced with SiCp at elevated temperatures. Mater Sci Eng A 364:296-304

[24] X.J. Wang, X.S. Hu, W.Q. Liu, J.F. Du, K. Wu, Y.D. Huang, M.Y. Zheng (2017) Ageing behavior of as-cast SiCp/AZ91 Mg matrix composites, Mater Sci Eng A 682:491–500

[25] K. B. lee, H. Kwon (2002) Strength of Al-Zn-Mg-Cu Matrix Composite Reinforced with SiC Particles. Metall Mater Trans A 33A:455-465

[26] A. Kumar, K. Pal, S. Mula (2017) Simultaneous improvement of mechanical strength, ductility and corrosion resistance of stir cast Al7075-2% SiC micro- and nano composites by friction stir processing. J Manuf Process 30:1–13

[27] O.B. Bembalge, S.K. Panigrahi (2019) Aging behavior of ultrafine-grained AA6063/SiC composites with varying reinforcement sizes. Mater Sci Eng A 768:138482

[28] T. Lu, W. Chen, W. Xu, P. Wang, M. Mao, Y. Liu, Z. Fu (2018) The effects of Cr particles addition on the aging behavior and mechanical properties of SiCp/7075Al composites. Mater Charact 136:264–271

[29] Z. Min, W. Gaohui, J. Longtao (2004) Aging behavior and precipitation kinetics of SiCp/6061AI composites. J Mater Sci 39:1759 – 1763

[30] Y. Liu, D. Jiang, B. Li, T. Ying, J. Hu (2014) Heating aging behavior of Al–8.35Zn–2.5Mg–2.25Cu alloy. Mater Des 60:116-124

[31] T. Hu, K. Ma, T.D. Topping, J.M. Schoenung, E.J. Lavernia (2013) Precipitation phenomena in an ultrafine-grained Al alloy. Acta Mater 61:2163-2178

[32] S. K. Panigrahi, R. Jayaganthan (2011) Effect of ageing on microstructure and mechanical properties of bulk, cryorolled, and room temperature rolled Al 7075 alloy. J Alloy Compd 509:9609– 9616

[33] R. Dong, W. Yang, Z. Yu, P. Wu, M. Hussain, L. Jiang, G. Wu (2015) Aging behavior of 6061Al matrix composite reinforced with high content SiC nanowires. J Alloy Compd 649:1037–1042

[34] C. Wu, K. Ma, D. Zhang, J. Wu, S. Xiong, G. Luo, J. Zhang, F. Chen, Q. Shen, L. Zhang, E.J. Lavernia (2017) Precipitation phenomena in Al-Zn-Mg alloy matrix composites reinforced with B_4C particles. Sci Rep 7:9589

[35] K. Kondoh, H. Fukuda, J. Umeda, H. Imai, B. Fugetsu (2014) Microstructural and mechanical behavior of multi-walled carbon nanotubes reinforced Al-Mg-Si alloy composites in aging treatment. Carbon 72:15–21

[36] Y. Zhao, X. Ma, X. Zhao, H. Chen, X. Liu (2017) Enhanced aging kinetic of Al_3BC/6061 Al composites and its micro mechanism. J Alloys Compd 726:1053–1061

[37] M. Legros, G. Dehm, E. Arzt, T.J. Balk (2008) Observation of giant diffusivity along dislocation cores. Science 319:1646–1649

[38] W. Chen, Y. Liu, C. Yang, D. Zhu, Y. Li (2014) (SiCp+Ti)/7075Al hybrid composites withhigh strength and large plasticity fabricated by squeeze casting. Mater Sci Eng A 609:250-254

List of Tables.

Table 1 Chemical analysis of 7075 Al alloy

Element	Al	Zn	Mg	Cu	Cr	Si	Fe
Wt%	89.87	5.5	2.6	1.5	0.2	0.15	0.18

Table 2 Rockwell hardness (HRB) values for AA 7075 and AA7075- SiCp 5 vol. % composite aged at 120ºC

Time (Hr)	Hardness value (HRB)	
	AA7075	AA7075-5 vol. % SiCp
0	35	31
0.5	75	62
2	79	79
24	84	89
40	86	86
48	85	84
72	82	82
96	83	81

Table 4 Exothermic and endothermic peak temperature of the as quench specimen of 7075 alloy-5 vol % SiC composite at different heating rate.

Heating rate (K/min)	**Peak temperatures**					
	I	**II**	**III**	**IV**	**V**	**VI**
5	75	118	218	232	270	402
10	84	137	227	255	274	410
15	92	144	237	259	285	412
20	94	148	240	270	290	413
25	97	152	244	273	295	415

Table 3 DSC thermogrm peak temperatures of as quench specimen AA7075 at different heating rates.

Heating rate (K/min)	**Peak Temperatures**					
	I	**II**	**III**	**IV**	**V**	**VI**
5	79	127	191	205	222	398
10	88	141	202	222	233	427
15	94	159	219	226	237	429
20	98	158	239		245	445
25	101	168	246	290	292	447

Table 5 Diffusion activation energies of AA7075 and AA7075-5 vol. % SiC composite

Specimen Name	Activation energies, kj/mol		
	GP formation	ή formation	η formation
AA7075	73.42	127.53	146.02
AA7075-5 vol. %SiC	69.89	117.65	139.6

a

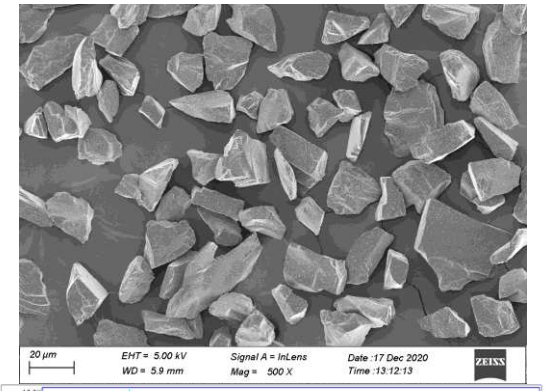

b

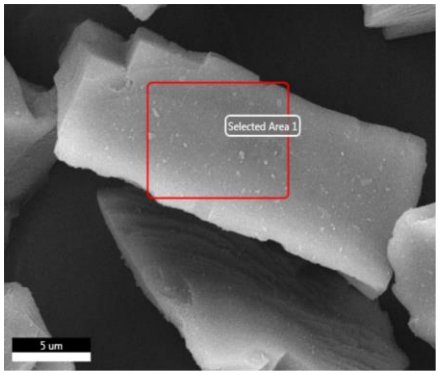

c

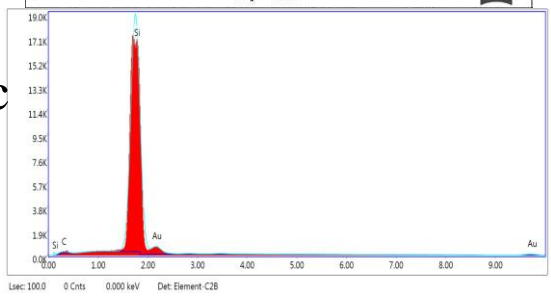

d

Element	Weight %	Atomic %
C K	17.15	35.09
SiK	72.74	63.65
AuL	10.12	1.26

e

f

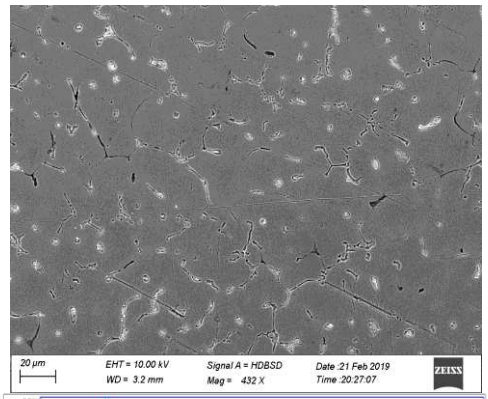

g

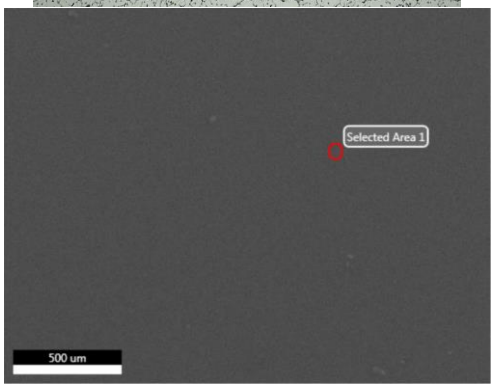

h

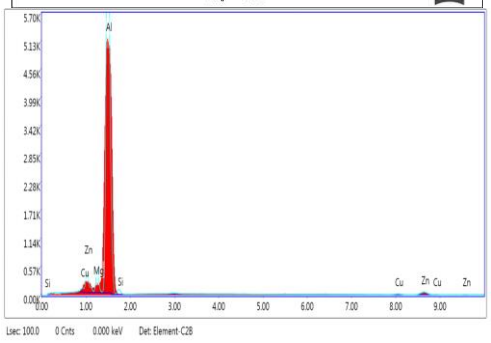

i

Element	Weight %	Atomic %
MgK	3.53	4.06
AlK	87.80	91.00
SiK	2.14	2.13
CuK	1.00	0.44
ZnK	5.52	2.36

Fig: 1 shows micrographs of as cast AA7075-5 Vol.% of SiC composite (a,b) optical micrograph, (c,d) SEM micrograph, (e,f) EDAX analysis.

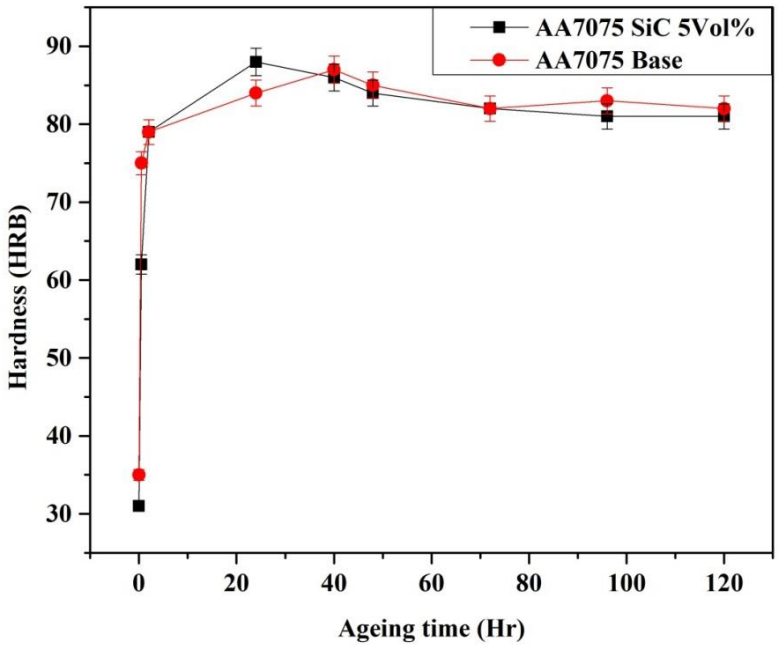

Fig: 2 Hardness of AA 7075 alloy and AA 7075 - 5 vol % SiC composite aged at 120^{o}C.

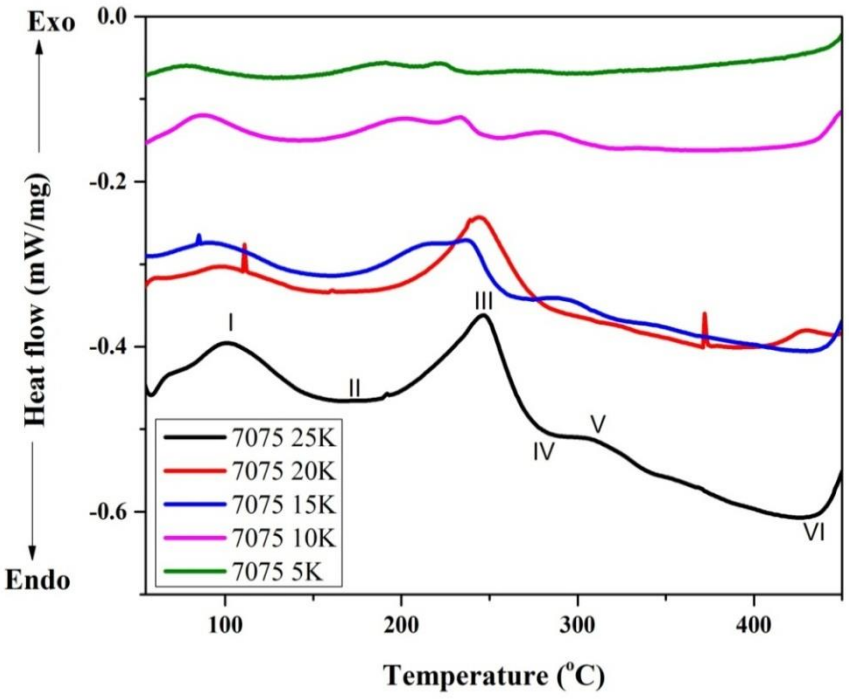

Fig: 3 Differential scanning calorimetry (DSC) curves of the as quench specimen AA7075 at different heating rate.

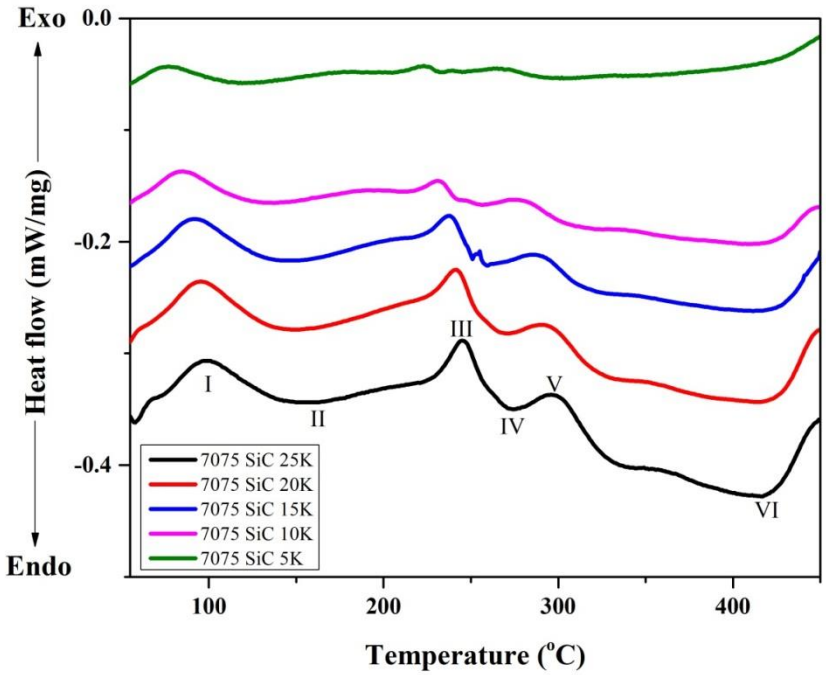

Fig: 4 Differential scanning calorimetry (DSC) curves of the as quench specimen AA7075-SiC with 5 vol. % of SiCp composite at different heating rate.

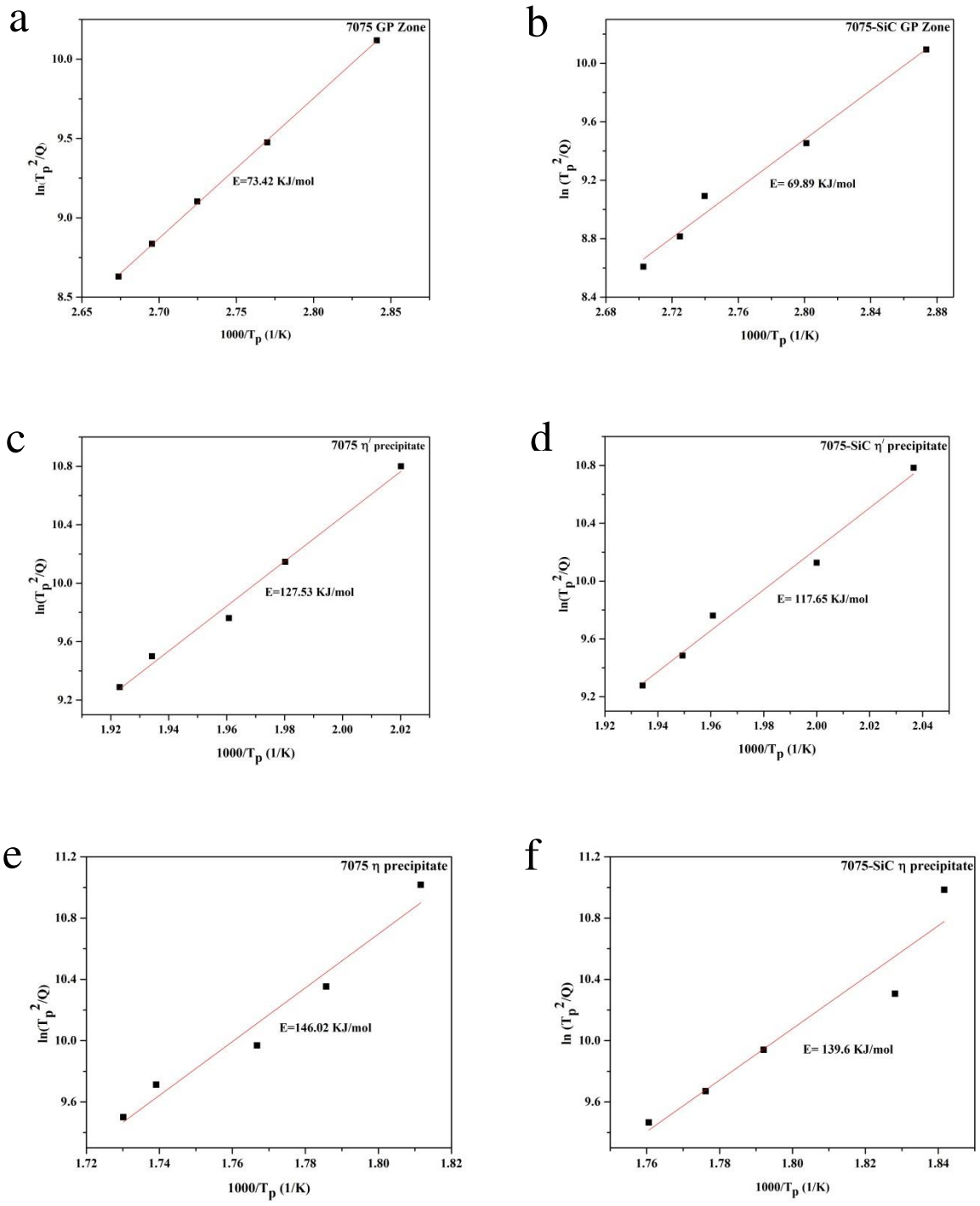

Fig: 5 Variations of ln (Tp^2/Q) with $1/T_p$ for the formation of GP zone, ή and η ($MgZn_2$) precipitates.

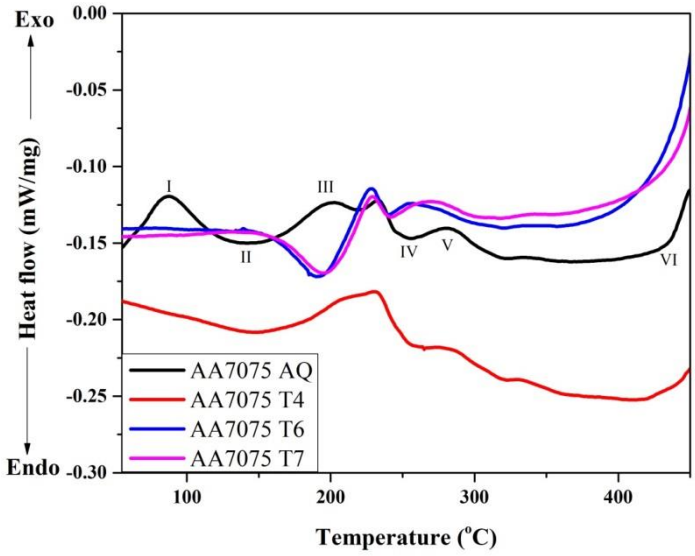

Fig: 6 DSC thermograms of AA7075 alloy of various tempers at heating rate of 10K/min

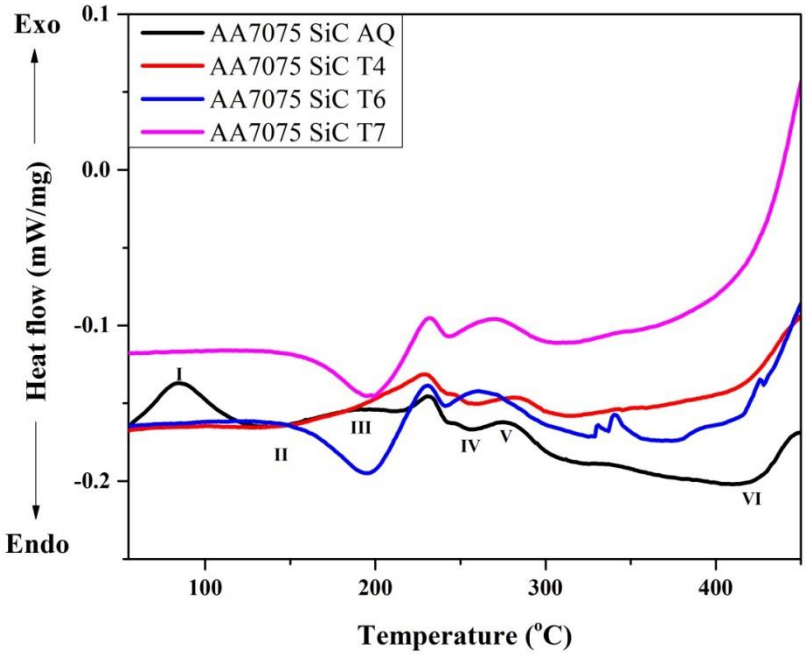

Fig. 7 DSC thermograms of AA7075-5 vol % SiCp composite of various tempers at heating rate of 10K/min.

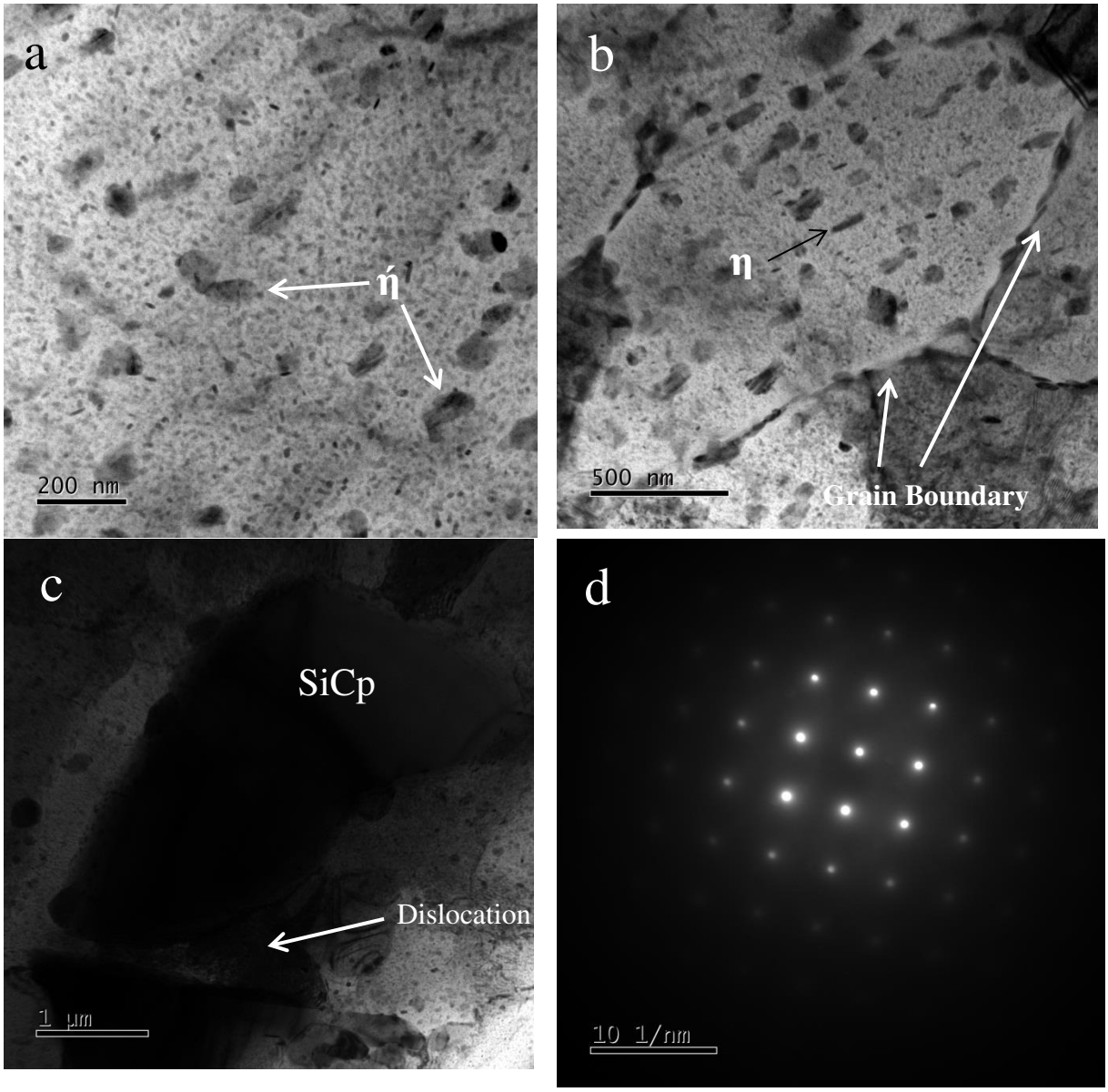

Fig. 8 TEM micrograph of the AA7075-5 vol. % SiCp of SiC particulate at (a)-(b) peak aged (T6) condion (d) SAED pattern.

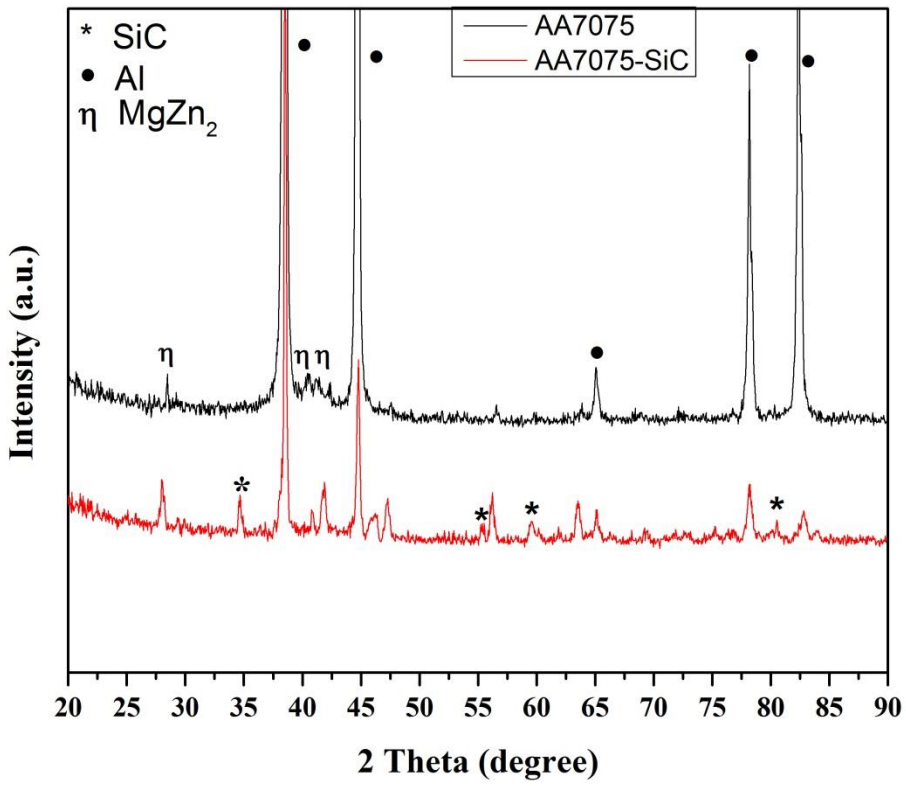

Fig. 9 XRD patterns of AA7075 and AA7075- SiC 5 vol. % composite of as cast sample.

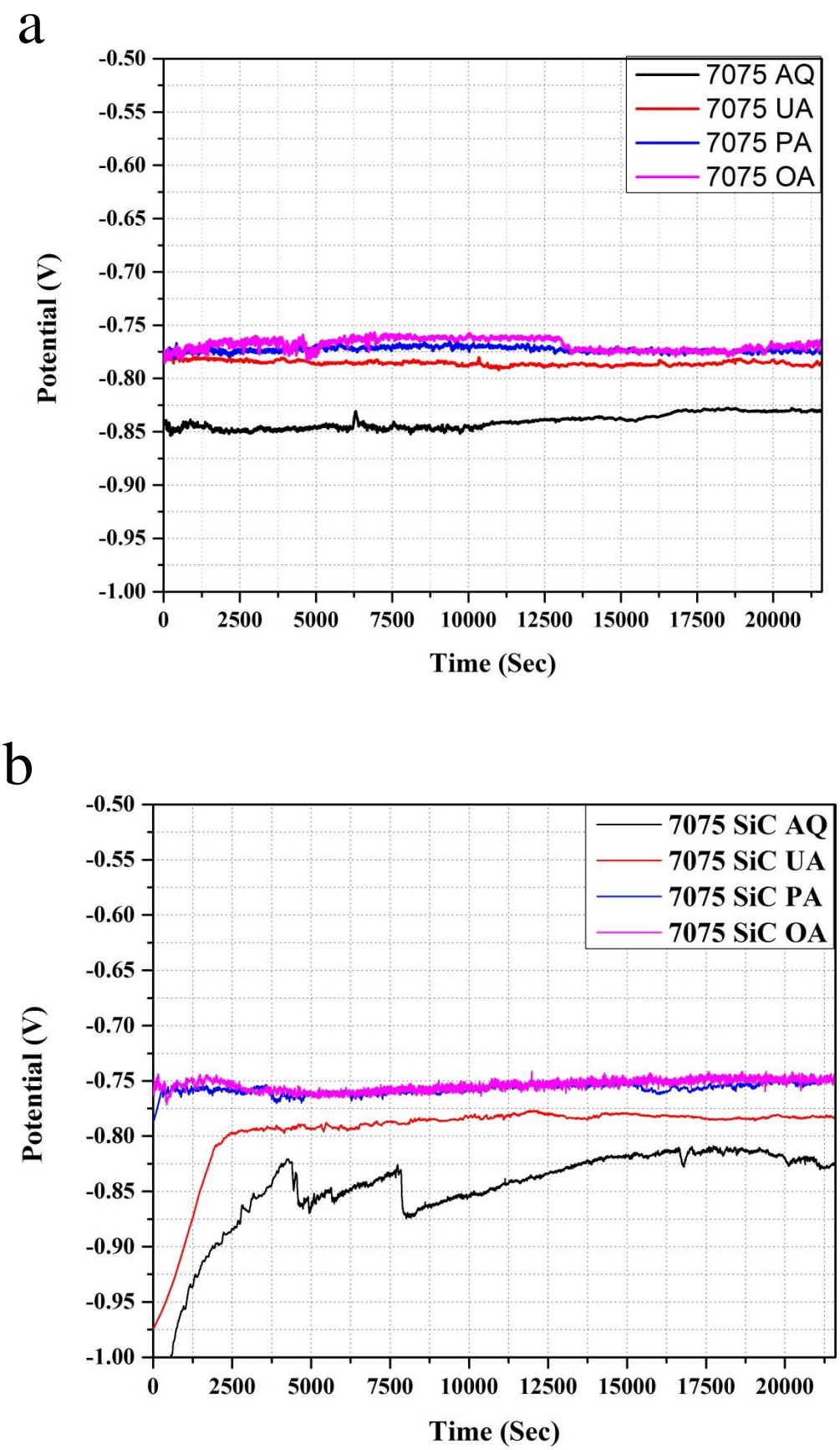

Fig. 10 variation of open circuit potential with time (a) AA7075 (b) AA7075- SiC 5 vol. % composite

Figures

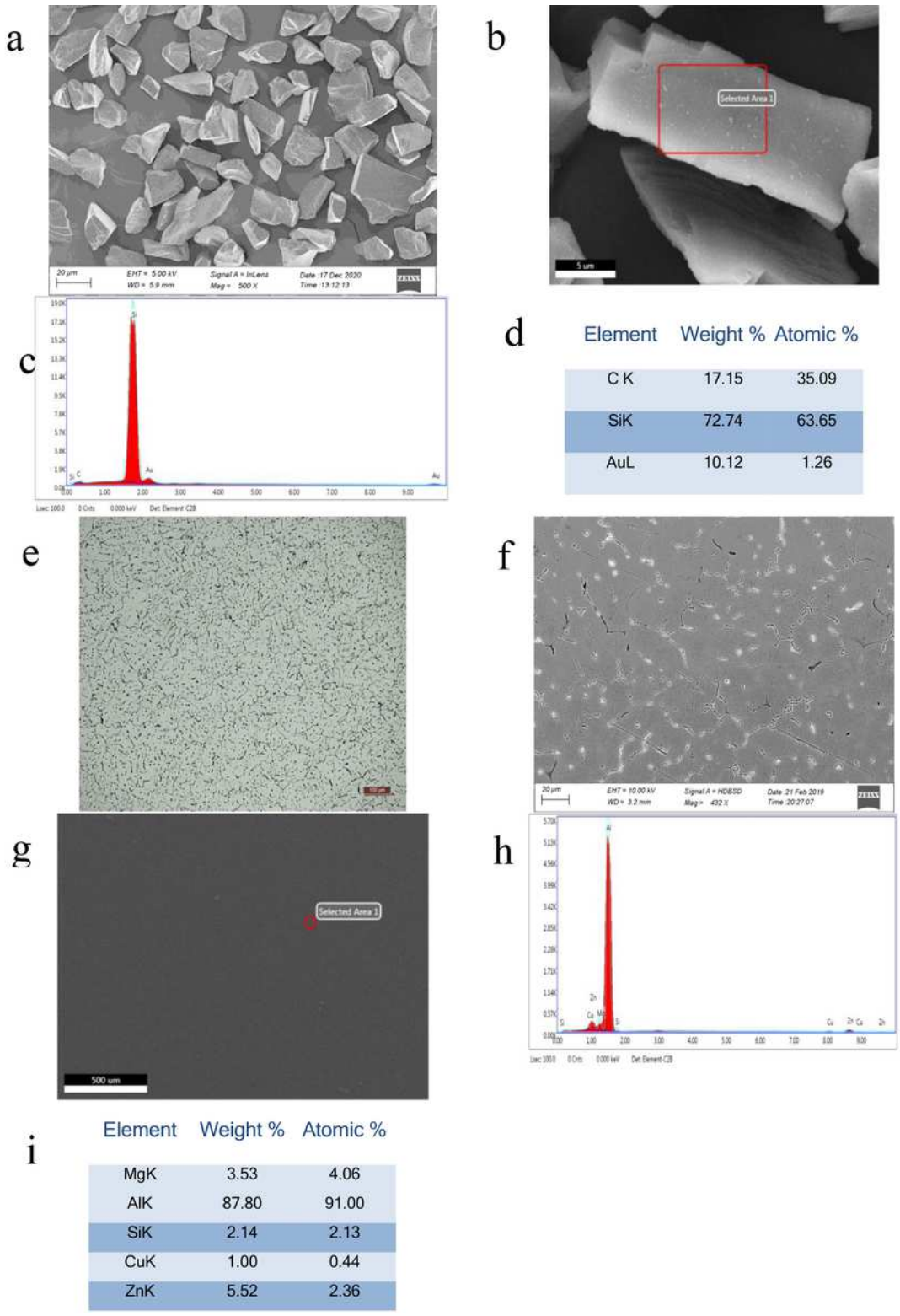

Element	Weight %	Atomic %
C K	17.15	35.09
SiK	72.74	63.65
AuL	10.12	1.26

Element	Weight %	Atomic %
MgK	3.53	4.06
AlK	87.80	91.00
SiK	2.14	2.13
CuK	1.00	0.44
ZnK	5.52	2.36

Figure 1

shows micrographs of as cast AA7075-5 Vol.% of SiC composite (a,b) optical micrograph, (c,d) SEM micrograph, (e,f) EDAX analysis.

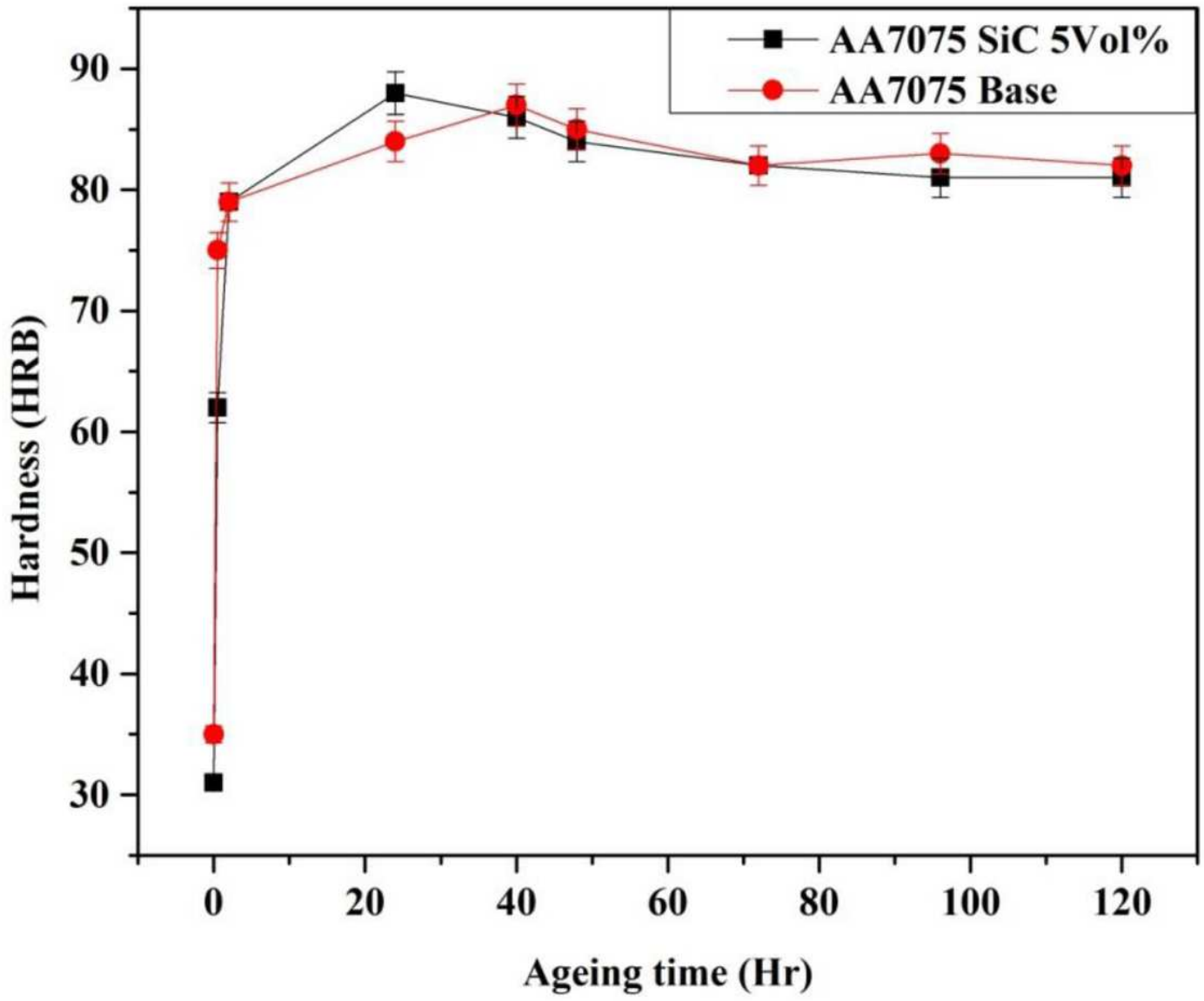

Figure 2

Hardness of AA 7075 alloy and AA 7075 - 5 vol % SiC composite aged at 120oC.

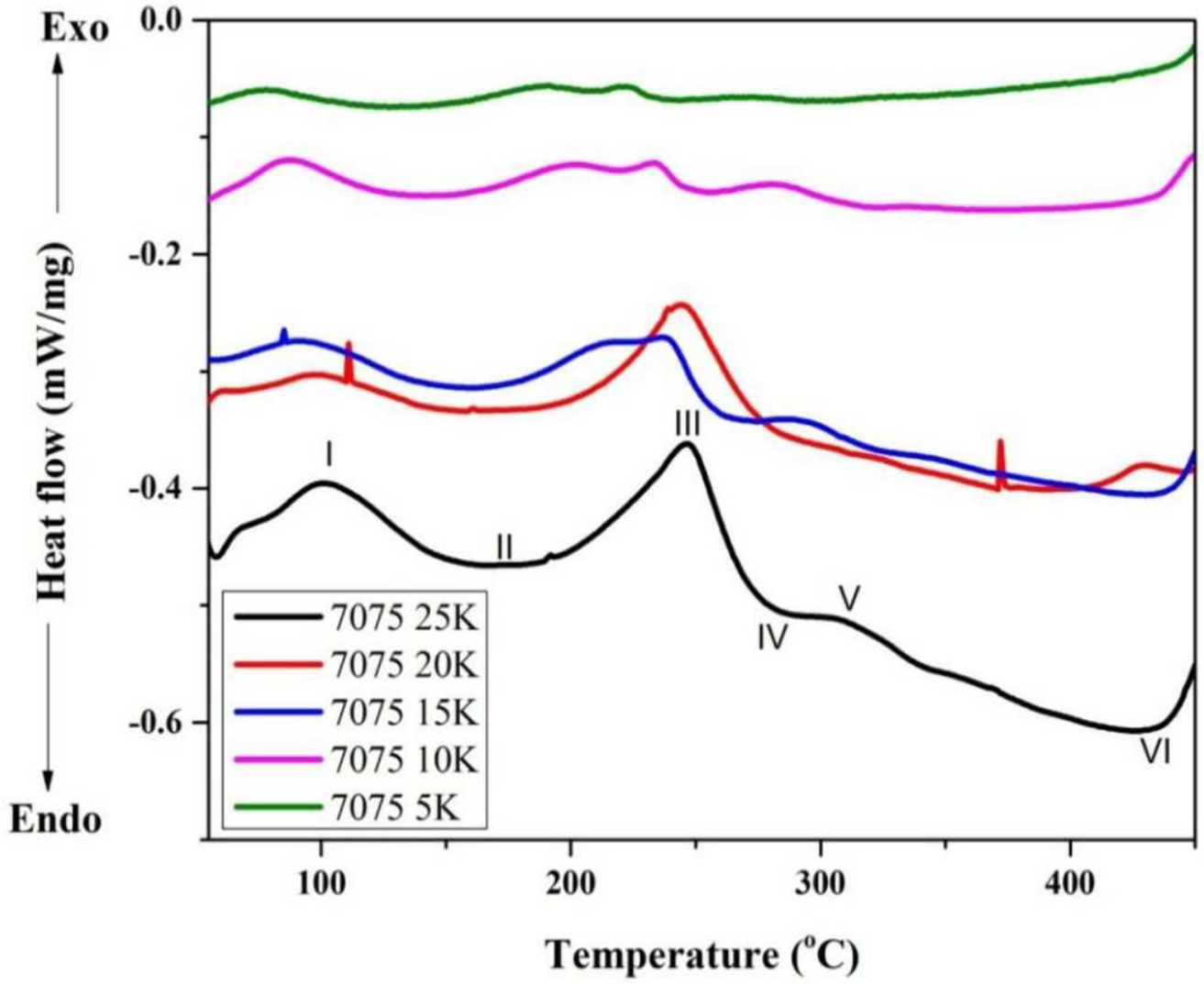

Figure 3

Differential scanning calorimetry (DSC) curves of the as quench specimen AA7075 at different heating rate.

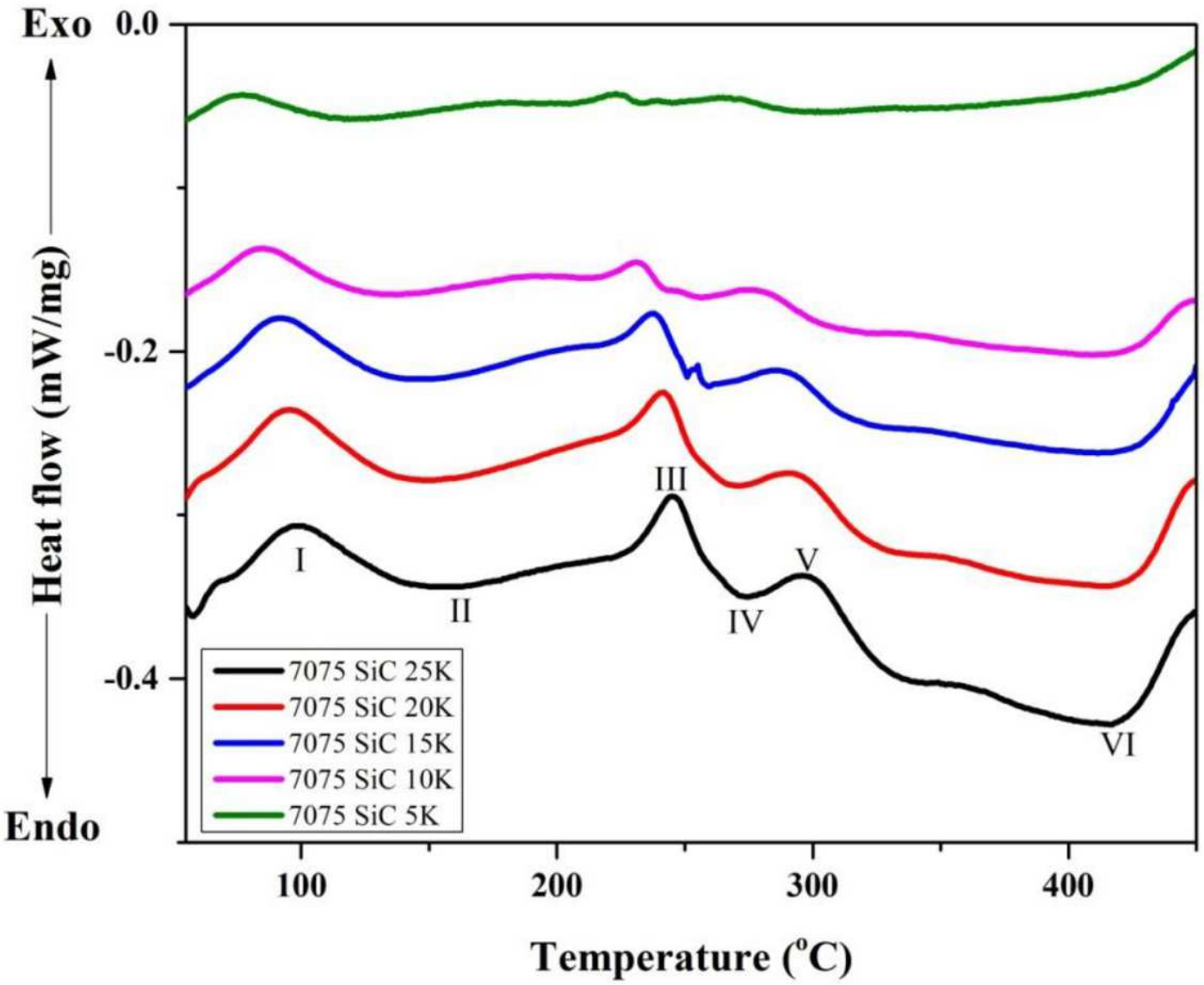

Figure 4

Differential scanning calorimetry (DSC) curves of the as quench specimen AA7075-SiC with 5 vol. % of SiCp composite at different heating rate.

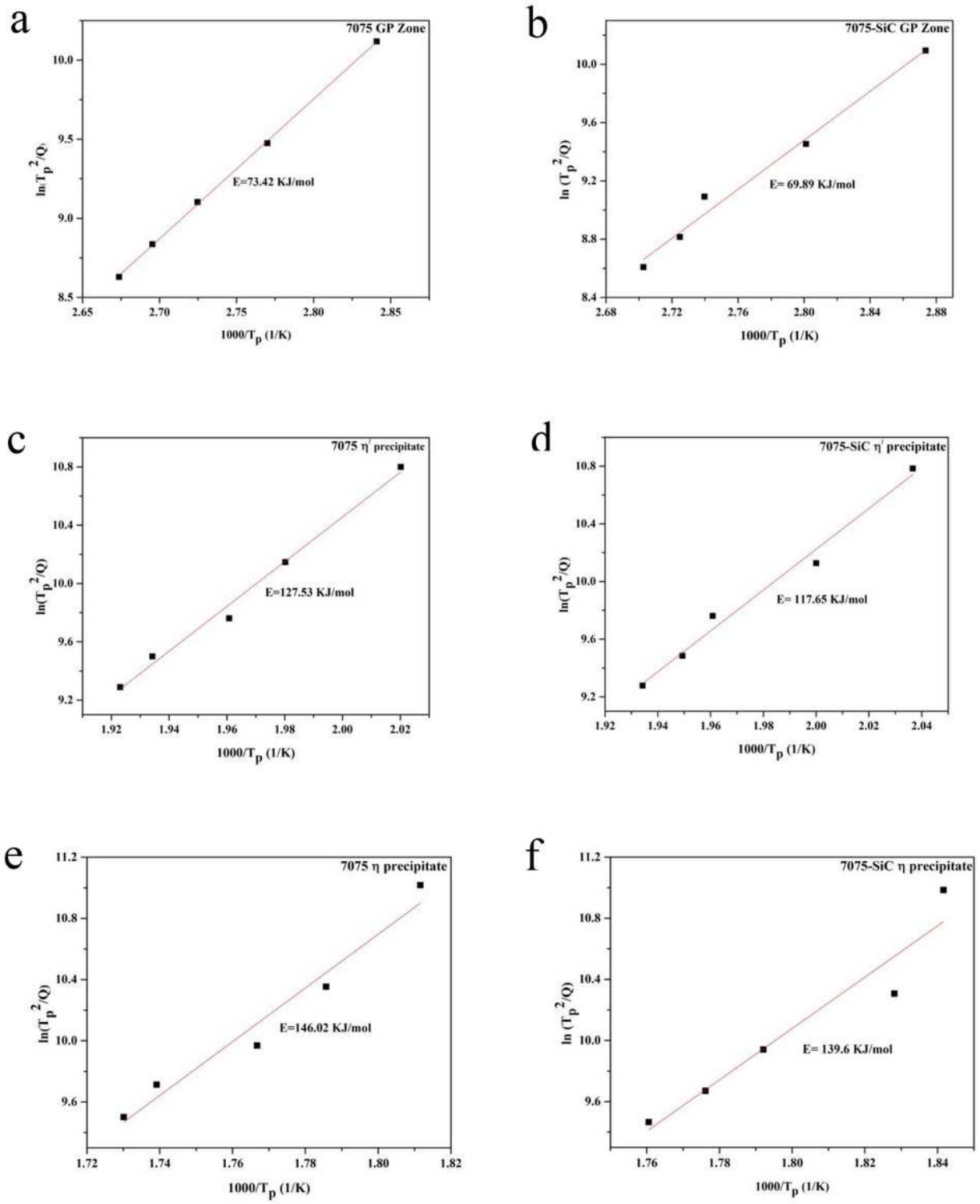

Figure 5

Variations of ln (Tp2/Q) with 1/Tp for the formation of GP zone, ή and η (MgZn2) precipitates.

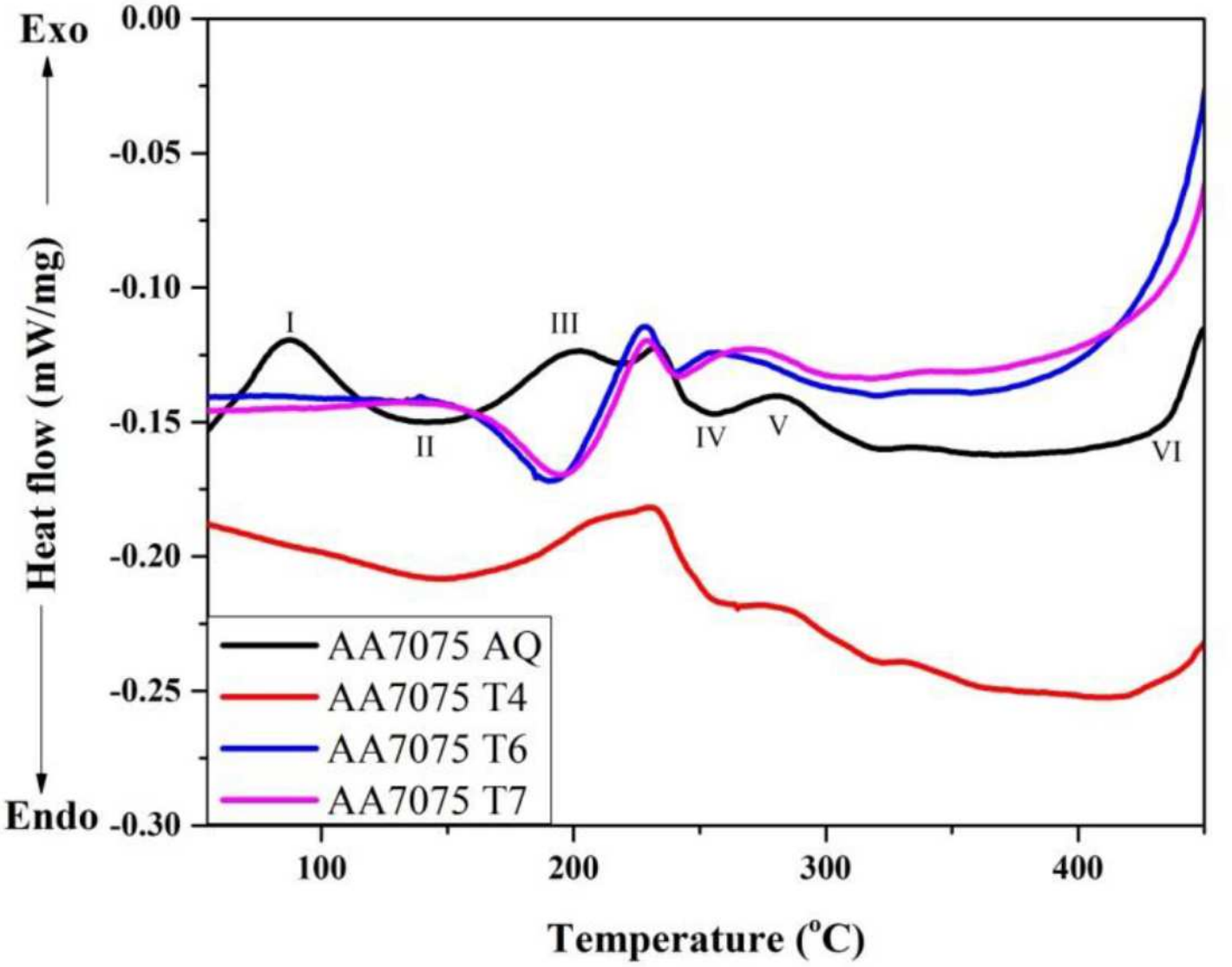

Figure 6

DSC thermograms of AA7075 alloy of various tempers at heating rate of 10K/min

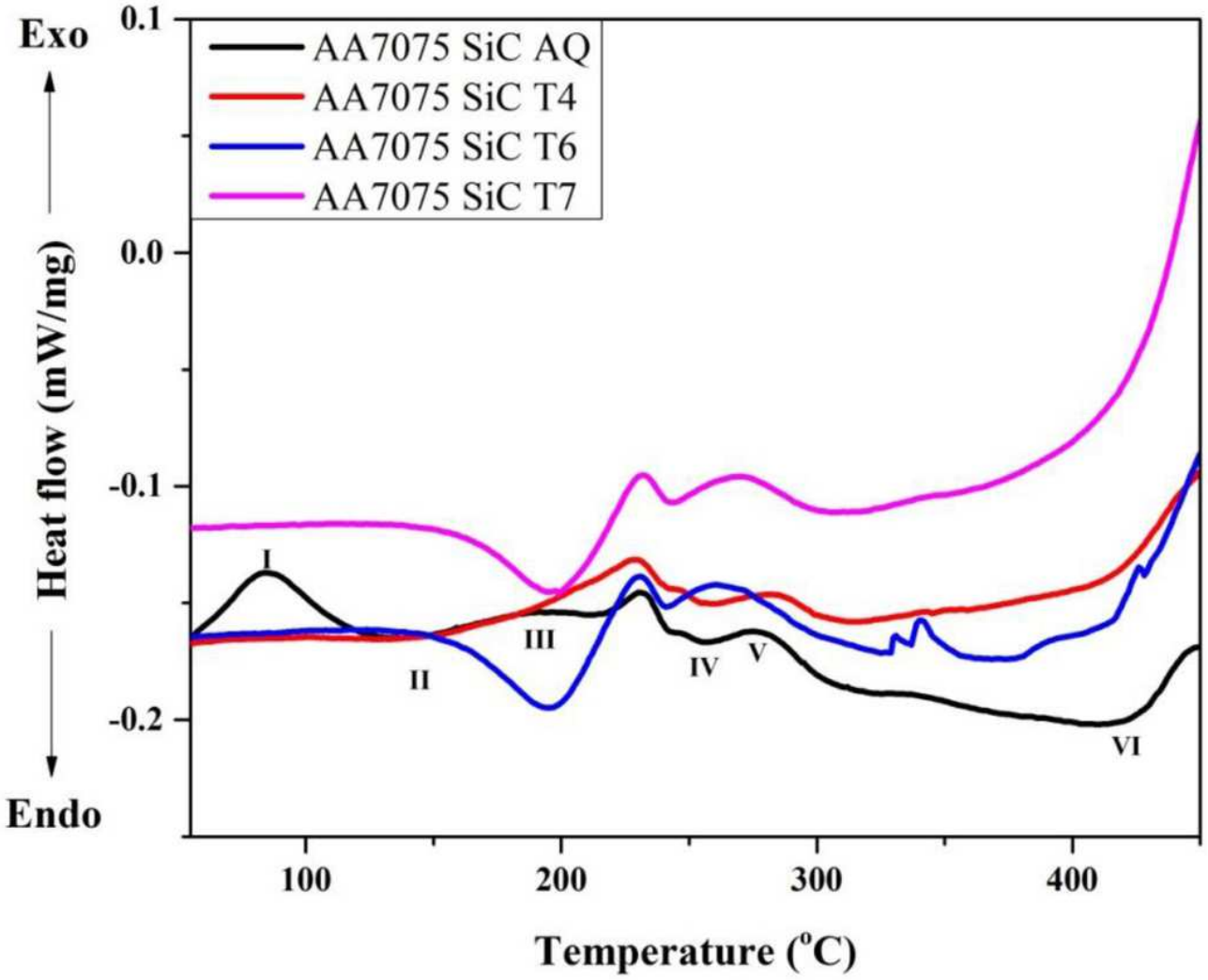

Figure 7

DSC thermograms of AA7075-5 vol % SiCp composite of various tempers at heating rate of 10K/min.

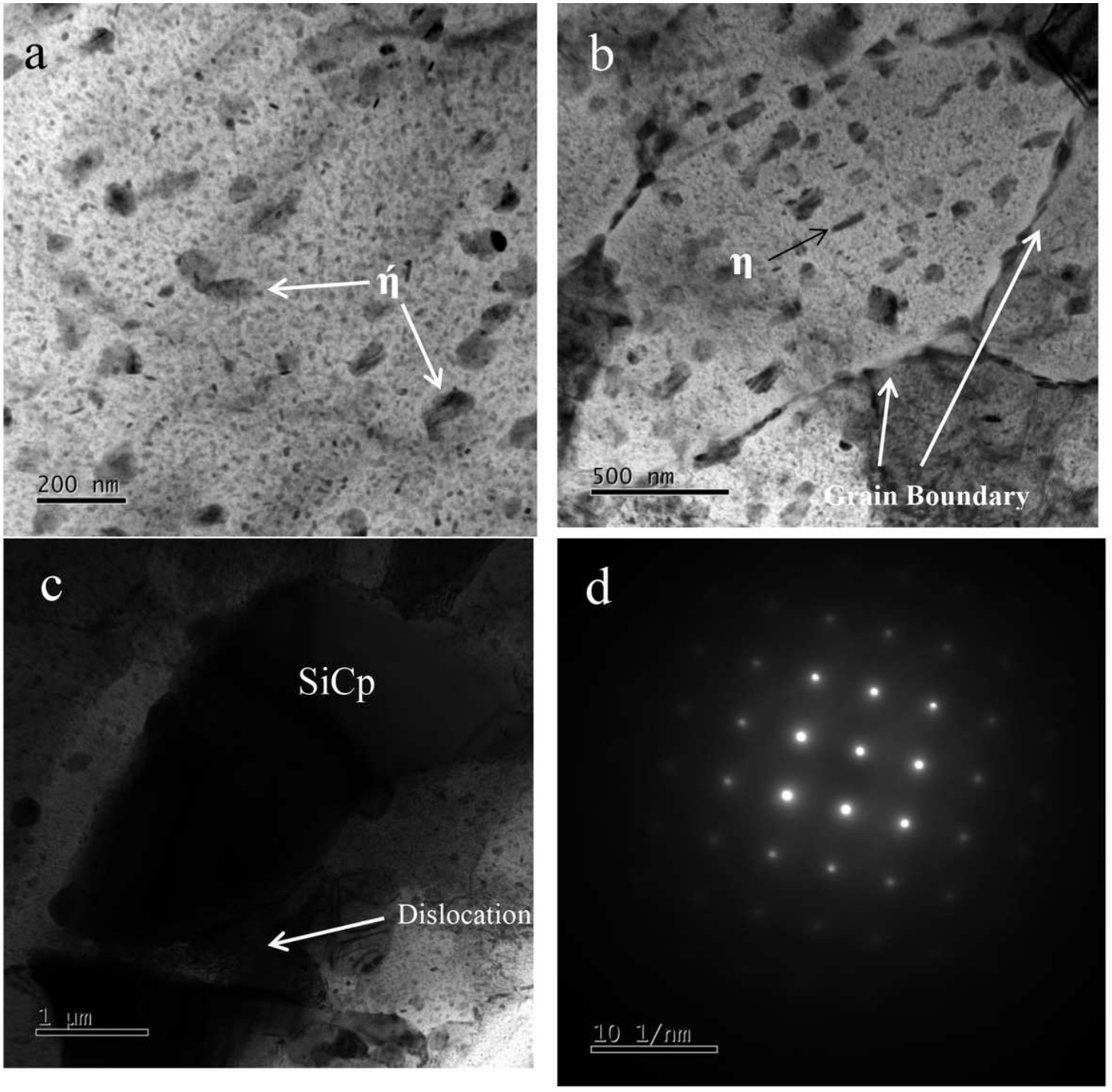

Figure 8

TEM micrograph of the AA7075-5 vol. % SiCp of SiC particulate at (a)-(b) peak aged (T6) condion (d) SAED pattern.

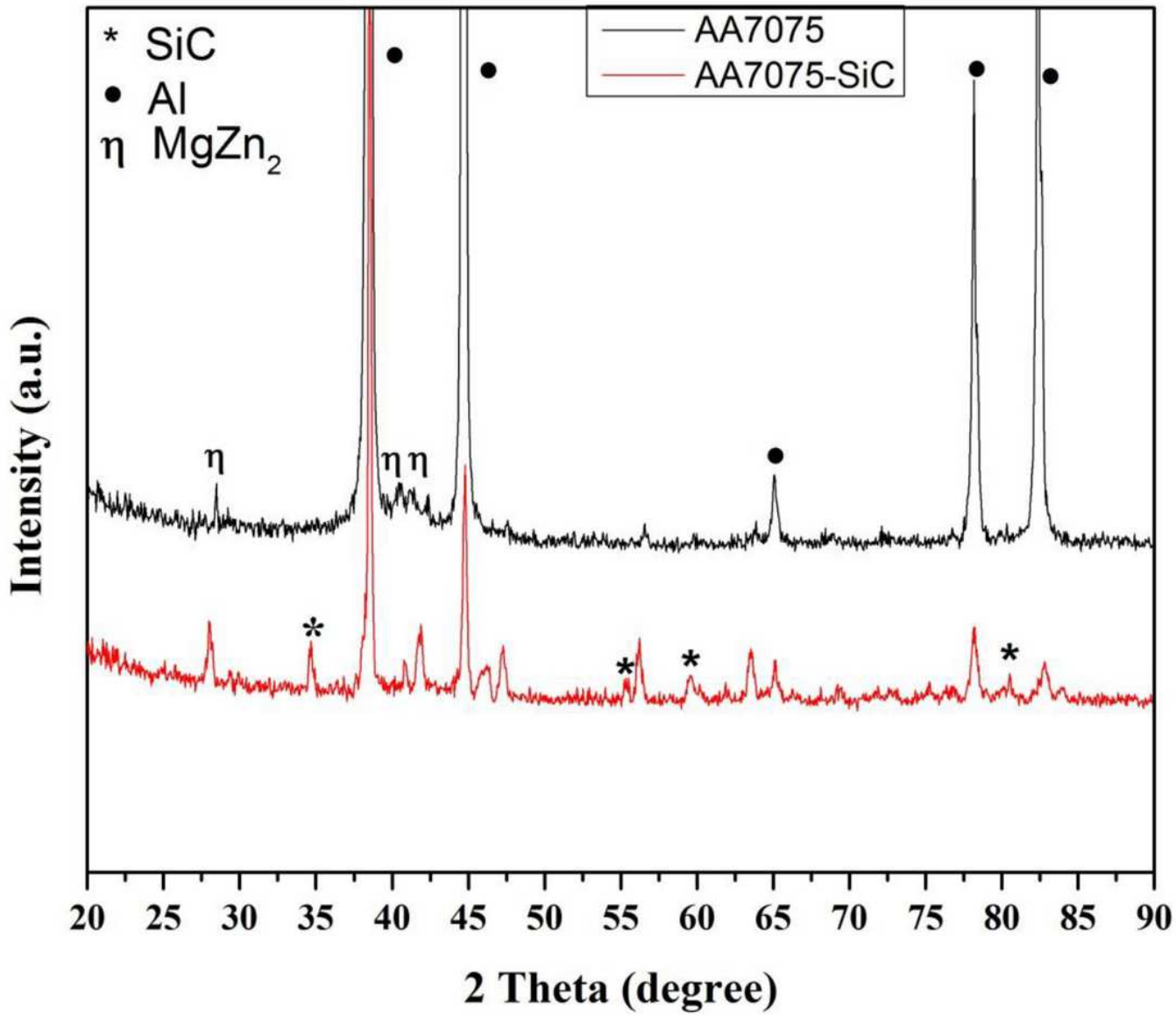

Figure 9

XRD patterns of AA7075 and AA7075- SiC 5 vol. % composite of as cast sample.

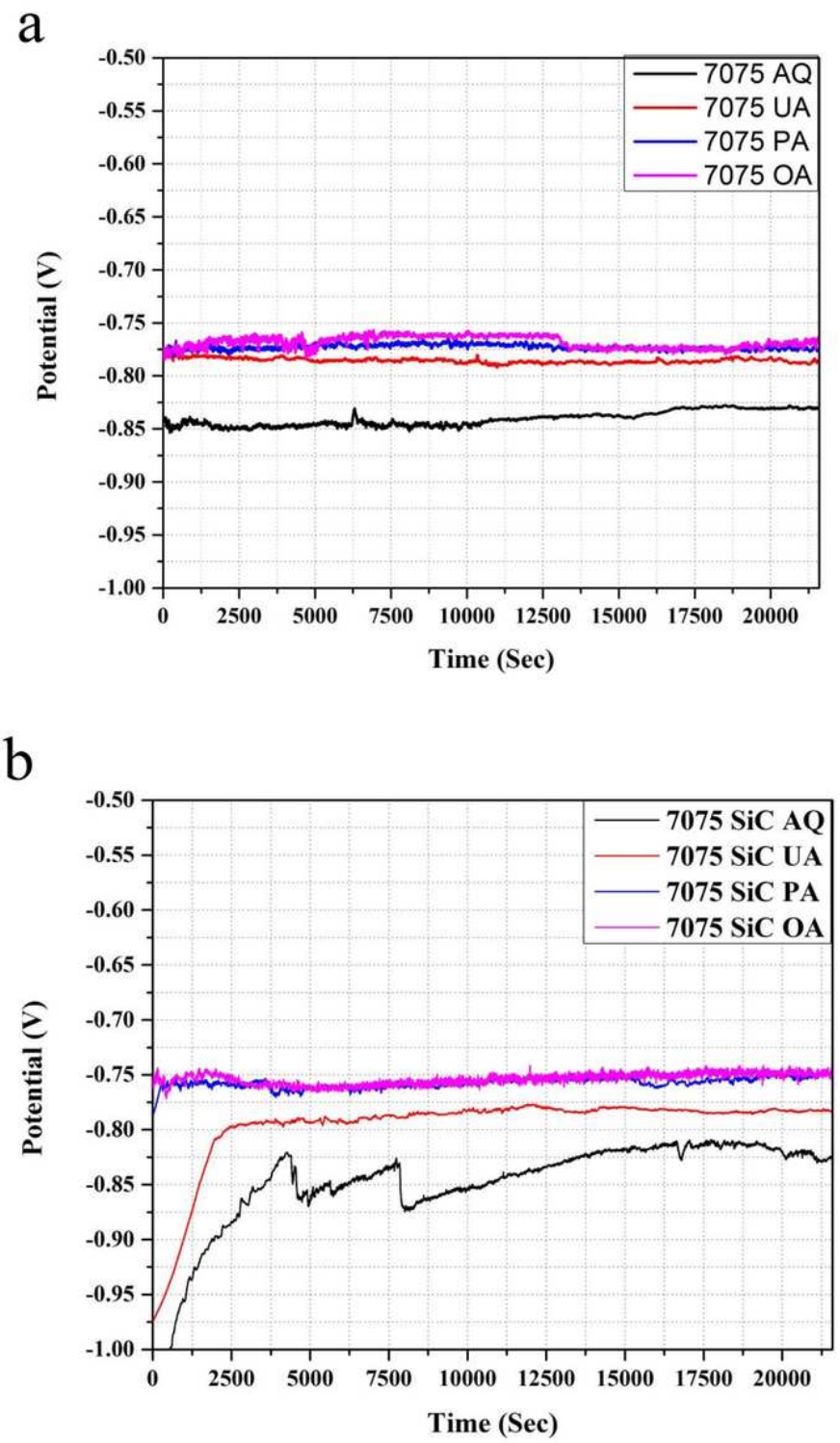

Figure 10

variation of open circuit potential with time (a) AA7075 (b) AA7075- SiC 5 vol. % composite